proposed antenna, probe feeding and an air gap (capacitive gap) were used. Simulations were conducted to optimize the lengths of the probe and air gap in order to obtain the widest bandwidth in terms of return loss (VSWR [lt] 2) at 2 GHz band. According to the measured results for the antenna implemented, the impedance bandwidth was 734 MHz (29.01%) ranging from 2.163 to 2.897 GHz and the axial ratio bandwidth (AR [lt] 3dB) was 135 MHz (5.48%) ranging from 2.394 to 2.529 GHz. The CP characteristic of the antenna can be applied to mobile applications for the 2.4 GHz WLAN.

REFERENCES

1. Z. Zhang, M.F. Iskander, J.C. Langer, and J. Mathews, Wideband Dipole Antenna for WLAN, Antenna Propagat Society Int Symp 2004 (2), 1963-1966.
2. M. Joseph, B. Paul, R.K. Raj, and P. Mohanan, Compact wideband antenna for 2.4 GHz WLAN, Electron Lett 40 (2004), 1460-1461.
3. H.J. Kim, S.M. Kim, J.M. Son, and W.G. Yang, Design and implementation of dual band circular polarization square patch antenna, Microwave Conf Proc 4 (2005), 2717-2720.
4. R. Garg, P. Bhartia, I. Bahl, and A. Ittipiboon, Microstrip antenna design handbook, Artech House, Norwood, MA, 2001.
5. A. Shackclford, K.F. Lee, D. Chatterjee, Small size wide bandwidth microstrip patch antenna, Antenna Propagat Soc Int Symp 1 (2001), 86-89.
6. M. Ali, T. Sittironnarit, V.K. Kunda, H.S. Hwang, R.A. Sadler, and G.J. Hayes, Wideband patch antenna for 5–6 GHz WLAN applications, Antenna Propagat Soc Int Symp 2 (2003), 930-933.
7. K.-L. Wong, F.-S. Chang, and T.-W. Chiou, Low-cost broadband circularly polarized probe-fed patch antenna for WLAN base station, Antenna Propagat Soc Int Symp 2 (2002), 526-529.
8. K.L. Lau and K.M. Luk, A novel wideband circularly polarized patch antenna based on L-probe and slot-coupling techniques, Antenna Propagat Soc Int Symp 3 (2003), 878-881.
9. H. Wong, P.Y. Lau, K.M. Mak, and K.M. Luk, Small circularly polarised folded patch antenna, Electron Lett 41 (2005), 1363-1364.
10. W.L. Stutzman and G.A. Thiele, Antenna theory and design, 2nd ed., Wiley, New York, NY 1998.
11. W.H. Kummer and E.S. Gillespie, Antenna measurements, Proc IEEE 66 (1978), 483-507.

THE RESONANT BEHAVIOR OF THE FIBONACCI FRACTAL TREE ANTENNAS

Basak Ozbakis and Alp Kustepeli
Department of Electrical and Electronics Engineering, Izmir Institute of Technology, 35430 Urla Izmir, Turkey; Corresponding author: basakozbakis@iyte.edu.tr

Received 21 August 2007

ABSTRACT: *An investigation of a novel fractal tree antenna with the application to two different geometries is presented. The antenna is designed by using the special Fibonacci number sequence which leads to nonuniform branch length ratios to form the fractal tree. This new approach gives better performance, especially in the miniaturization of the antenna, when compared with the conventional designs. The results obtained from the experiments are also compared with the computed ones and there is a very good agreement between the numerical and measured data.* © 2008 Wiley Periodicals, Inc. Microwave Opt Technol Lett 50: 1046–1050, 2008; Published online in Wiley InterScience (www.interscience.wiley.com). DOI 10.1002/mop.23299

Key words: *fractal tree antennas; Fibonacci sequence; resonant frequency*

1. INTRODUCTION

Fractal geometry is first defined by Benoit Mandelbrot in 1975 to describe complex geometries [1] and it is generated with an iterative procedure. An initial structure called generator is copied many times at different scales, positions, and directions [2] resulting fine, regular, or irregular configurations. There are a lot of different fractal geometries. Koch curves, Koch and Minkowski loops, Sierpinski triangles or carpets can be given as the best known examples for these kinds of structures. The most important property of fractal shapes is that they are self-similar structures and therefore their scaled versions have the same characteristics with the whole object.

Fractals have been recently used in antenna designs to obtain various kinds of small and multiband antennas [3–14]. Generally, the properties of the fractal geometry are related with the electromagnetic behavior of the antennas. As for the Koch fractal dipole antenna, if the heights of the antennas are fixed and the number of iterations is increased the resonant frequency of the antennas decreases. Decreasing the resonant frequency with fixed height has the same effect as miniaturizing the antenna at a fixed resonant frequency. In addition to the miniaturization effect, using fractals improves the antenna parameters, making them suitable for many applications. Most of the fractal antennas can also be used as multiband and wideband antennas because of the self-similar property of the geometry. Sierpinski antenna is one of those which can be used to achieve similar radiation patterns at various operating frequency bands.

When small and multiband antennas are considered, fractal trees are also very good candidates [15, 16]. They are widely used in the design of miniaturized antennas because of their space filling ability, compact size, and multiband behavior. Three dimensional fractal trees with self-similar branch structure are also examined in [17, 18]. Fractal tree antennas are designed by using various scale factors [19] but the length ratios of consecutive branches are constant. In this study, the antennas with nonuniform branch length ratios are proposed and investigated. The new antennas are compared with the ones designed by using uniform length ratios in terms of the fundamental antenna parameters. The antennas are also fabricated and measured.

2. ANTENNA DESIGN

Fractal tree antennas generated by applying an iterative procedure are obtained by using a constant scale factor and this factor in the designs is generally chosen as 1/2. Therefore, the branch lengths increases according to the number sequence 1, 2, 4, 8, 16, 32, $\cdots$ from the tip of the antenna to its base. Since the length of the following branch is the double of the previous one, the antenna is called as the D version in this work. The new antenna whose branch length ratios are not constant is designed similar to the D version but its branch lengths increases according to the Fibonacci number sequence from the tip to the base. The Fibonacci numbers appear in many unexpected places in nature such as on flowers, plants, and trees [20]. Therefore, in this study, it is intended to use this special sequence for the generation of fractal trees. The Fibonacci numbers are determined by the recurrence relation

$$F_n = F_{n-1} + F_{n-2}, \quad n > 2 \quad \text{and} \quad F_2 = F_1 = 1 \tag{1}$$

which leads to a sequence as 1, 1, 2, 3, 5, 8, $\cdots$. The novel design obtained from this sequence is called as the Fibonacci fractal tree

TABLE 1 The Branch Length Ratios for the *D* and *F* Versions

D_0	F_0	D_1	F_1	D_2	F_2	D_3	F_3	D_4	F_4	D_5	F_5
1/1	1/1	1/3	1/2	1/7	1/4	1/15	1/7	1/31	1/12	1/63	1/20
		2/3	1/2	2/7	1/4	2/15	1/7	2/31	1/12	2/63	1/20
				4/7	2/4	4/15	2/7	4/31	2/12	4/63	2/20
						8/15	3/7	8/31	3/12	8/63	3/20
								16/31	5/12	16/63	5/20
										32/63	8/20

antenna and it is designated by the *F* version. The branch length ratios of *D* and *F* versions obtained by the sequences are given in Table 1. In the table, the first and second columns for each iteration correspond to *D* and *F* versions, respectively. The resulting geometries for the tree structures are shown in Figure 1 for both of the narrow and wide configurations. The angles between the branches for all cases are always equal to 60°. In the narrow structure, the branches are close to each other. Since the branches are close, there are some touching branches in the new design after the first iteration and an interesting configuration for the antenna is obtained because of the special sequence. The branches are apart from each other in the wide structure as seen from the figure. In this configuration, the following branches are formed by splitting them with an angle of 30° to the left and right. Wide fractal tree antennas are examined to investigate the effect of the geometry in decreasing the resonant frequency.

3. NUMERICAL RESULTS AND DISCUSSIONS

In the numerical analysis, dipole antennas are considered and the results of the new design are compared with those of the *D* version. All of the computations are performed by using the SuperNEC 2.7 Academic version [21]. The lengths from the base to the tips for the structures shown in Figure 1 are always equal to 3.75 cm and the radius of wires is 0.075 mm for all cases. The resonant frequencies and the percent frequency shifts of the fractal tree antennas are given in Table 2 for the narrow and wide structures. The percent shift is calculated by comparing the frequency shift of

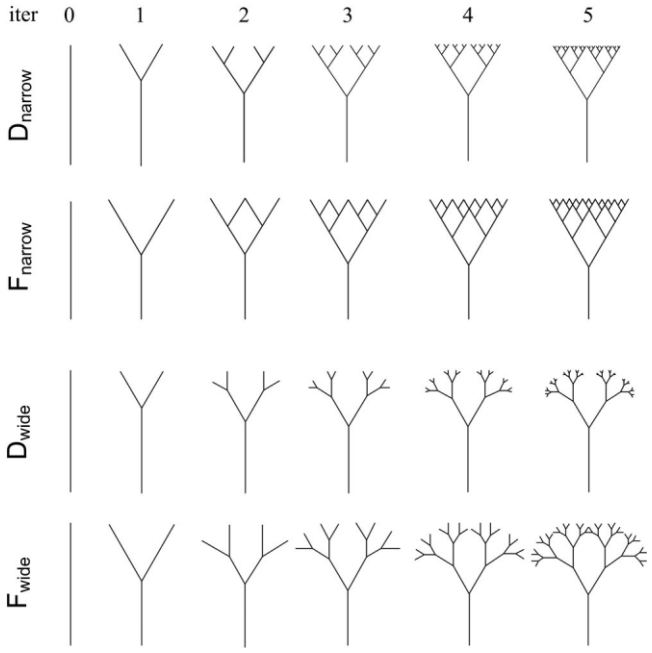

Figure 1 The configurations for the fractal tree antennas

TABLE 2 The Resonance Frequencies and the Percent Shifts for the Antennas

	Narrow Antennas			Wide Antennas		
itr	f_{D_i}	f_{F_i}	% Shift	f_{D_i}	f_{F_i}	% Shift
0	1900	1900	—	1900	1900	—
1	1590	1550	13	1590	1550	12.9
2	1400	1350	10	1392	1308	16.5
3	1300	1250	8.3	1262	1168	14.7
4	1245	1195	7.6	1174	1065	15
5	1200	1155	6.4	1125	1000	16.1

the proposed antennas and the frequency shift of the *D* version with respect to the straight dipole. The formula used in the calculations can be expressed as

$$\frac{f_{D_i} - f_{F_i}}{f_{\text{sd}} - f_{D_i}} \tag{2}$$

where f_{D_i} and f_{F_i} are the resonant frequencies of the *D* and *F* versions at the i^{th} iteration, respectively, and f_{sd} is the resonant frequency of the straight dipole which is 1900 MHz. The resonant frequencies of the narrow and wide antennas decrease while the iteration number increases. As seen from the table, the wide antennas have better performance than the narrow antennas. The resonant frequency difference for the narrow and wide configuration of *D* version is small at lower iterations while the difference reaches 75 MHz at the fifth iteration. For the *F* version, the difference is approximately the twice of the ones for *D* version and reaches 155 MHz at the last iteration. The resonant frequency difference between D_5 and F_5 for the narrow one is 45 MHz while the difference between the wide D_5 and F_5 antennas is 125 MHz. For a better determination of performances, the percent shift of resonant frequencies must be examined. For narrow configurations, the proposed antenna gives good results but for the wide one the performance of the antenna is remarkable. The resonant frequency at the fifth iteration decreases to 1000 MHz which is approximately the half of the resonant frequency of straight dipole and the shift reaches to 15–16% even from the first iterations. Consequently, it can be seen that the *F* antennas are more effective in decreasing resonant frequency when compared with the standard *D* version. Another interesting result can be observed from

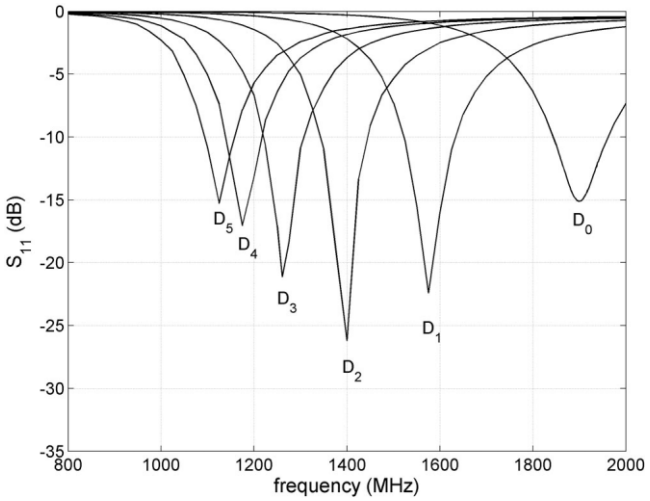

Figure 2 The input reflection coefficients for the *D* versions

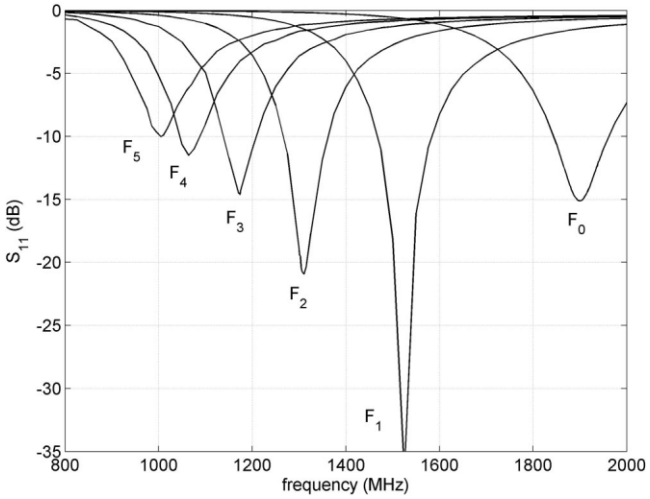

Figure 3 The input reflection coefficients for the *F* versions

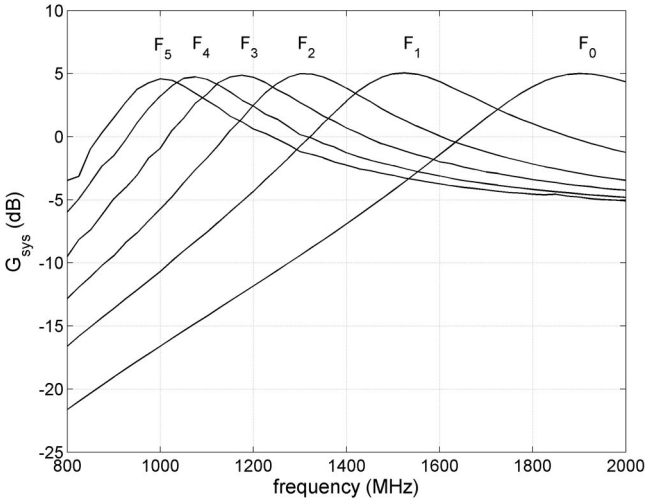

Figure 5 The system gains for the *F* versions

the table that the narrow *F* antennas have nearly the same performance with the wide configuration of *D* version in decreasing resonant frequency. If the resonant frequencies of the wide antennas are carefully examined one can also see that the resonant frequencies of F_4 and F_3 antennas are smaller than those of D_5 and D_4 antennas, respectively, and for the narrow ones they are about to be equal. From the above information, it can be concluded that the same performance of the *D* version can be obtained by the *F* version at lower iterations with simpler configurations. Since the branches closer to the tips are very small at higher iterations, obtaining the same performance with simpler geometries and at lower iterations becomes more important. To give an idea about the input reflection, the computed S_{11} values of wide *D* and *F* antennas are given in Figures 2 and 3, respectively. The system gain of antennas (G_{sys}) is another important parameter and must be examined in the designs. The system gain can be calculated by using the following formula

$$G_{sys}(dB) = G_{ant}(dB) + 10\log(1 - |\Gamma|^2), \tag{3}$$

where G_{ant} is the antenna gain and Γ is the input reflection coefficient. After computing G_{ant}, the system gain can be obtained by using the values given in Figures 2 and 3 via the Eq. (3). The overall system gains for the antennas are presented in Figures 4 and 5. They are similar to each other and their picks occur at the resonant frequencies of the antennas. Since the resonant frequencies shift, the system gains shift accordingly. The quality factor (*Q*) is another antenna parameter and it is generally considered in the antenna designs. The quality factor is defined as the ratio of the stored electric energy (W_e) or magnetic energy (W_m) to the radiated power (P_{rad}). There is a fundamental limit value (Q_{limit}) for every antenna structure and it can also be calculated easily [3, 4]. The quality factors for the wide antennas are shown in Figures 6 and 7. In the figures, the Q_{limit} value of antennas is also presented. The overall quality factor of the antennas is decreasing while the iteration number increases which means it gets better at higher iterations. Although it seems there is not much difference between the *Q* values of the antennas, the *F* version is again more effective in decreasing the quality factor than the *D* version. The far field patterns of D_5, F_5 and $F_0(D_0)$ versions at their resonant frequencies are also shown in Figure 8 and they are omnidirectional in the azimuth plane. There is not any difference between the patterns of D_5 and F_5 versions, and they are also very close to that of F_0 version. The radiation patterns of the antennas are not affected

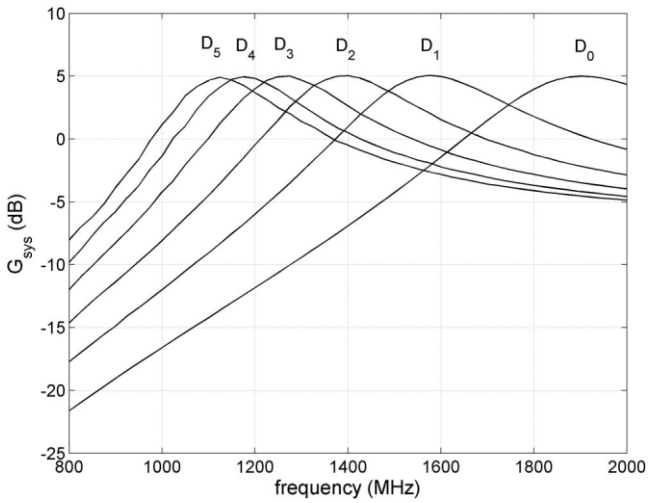

Figure 4 The system gains for the *D* versions

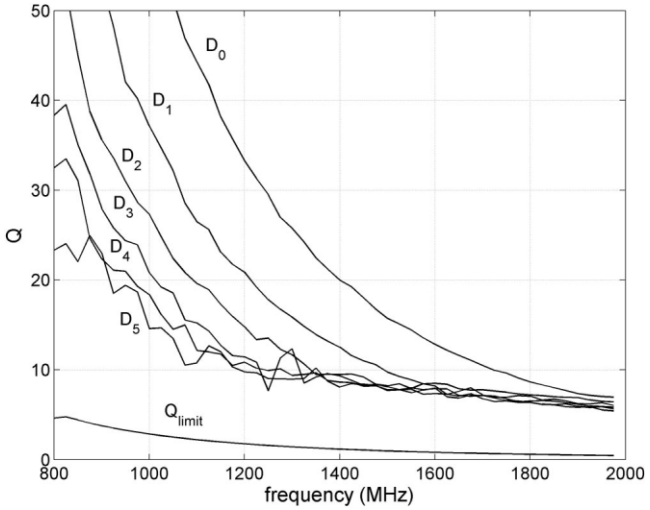

Figure 6 The quality factors for the *D* versions

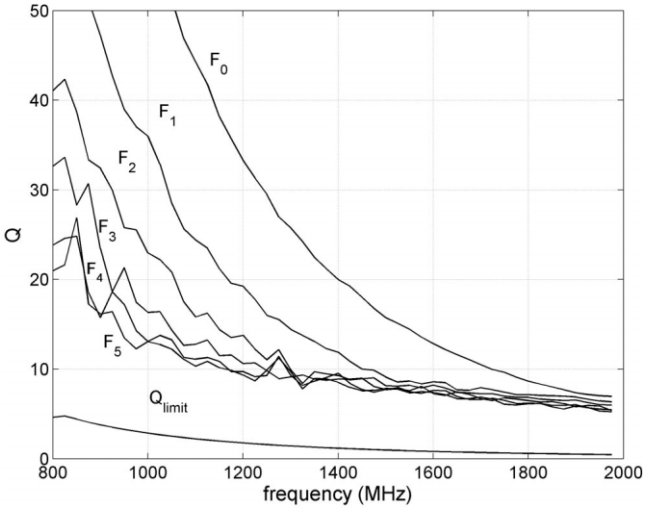

Figure 7 The quality factors for the *F* versions

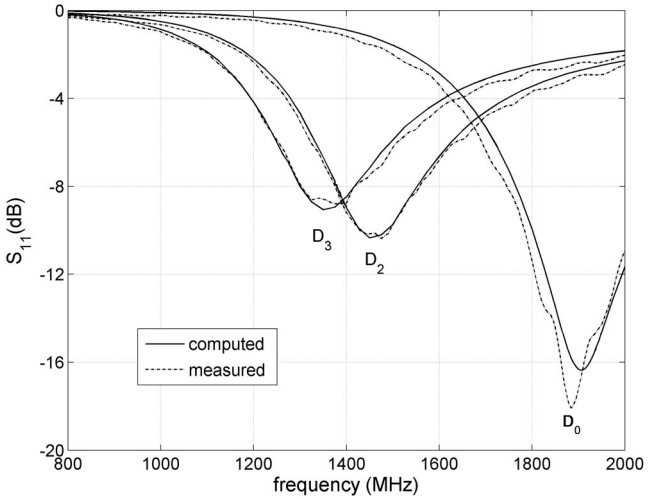

Figure 9 The measured and computed S_{11} for the *D* versions

from the branch length ratios and the geometry of the fractal tree antennas.

To obtain a different tree configuration the Fibonacci numbers can be modified by leaving the first one out of the sequence and a new recurrence relation

$$F_{m_n} = F_{m_{n-1}} + F_{m_{n-2}}, \quad n > 2 \quad \text{and} \quad F_{m_2} = 2, F_{m_1} = 1 \qquad (4)$$

can be obtained. The modified sequence then becomes as 1, 2, 3, 5, 8, 13, 21, $\cdots$. The fractal tree antennas formed by the use of this sequence in the design procedure were also investigated in this study. The results obtained are again better than those of the *D* version. Although they are close to the ones for the *F* version, the *F* antennas always give the best results.

From the discussions above, it is seen that the same or better performance in terms of the fundamental antenna parameters is obtained with the *F* version at lower frequencies when compared with the *D* and F_m versions. Therefore, one can conclude that the antennas can be made smaller with at least the same or better performance by using the proposed *F* antenna.

4. EXPERIMENTAL STUDY

Experimental study was performed by using the monopole antennas. Wide configurations of the D_2, D_3, F_2, and F_3 versions and the straight monopole which corresponds to the F_0 or D_0 versions were fabricated and measured. The antennas were mounted on brass plates with an area of 70 $\times$ 70 cm^2 and their lengths from the tips to the base are equal to 3.75 cm as chosen in the numerical study. They were fed by using 85 mil semirigid coaxial cables and SMA connectors were used at the other side of cables for the connection to the network analyzer. The radius of wires used to fabricate the monopoles was chosen as to be equal to that of the center conductor of coaxial cable which is 0.254 mm. The measured and computed values of input reflection coefficient (S_{11}) for the *D* and *F* version of the antennas are presented in Figures 9 and 10, respectively. As can be seen from the figures, the measured and computed results are in a very good agreement.

5. CONCLUSION

A novel fractal tree antenna, called Fibonacci fractal tree antenna, has been designed and introduced in this article. The main differ-

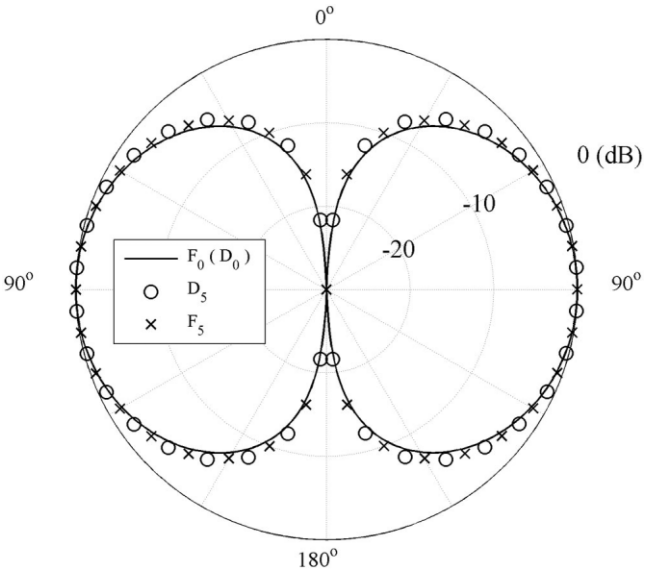

Figure 8 The far field patterns of the F_5, D_5, and F_0 (D_0) versions at the resonant frequencies

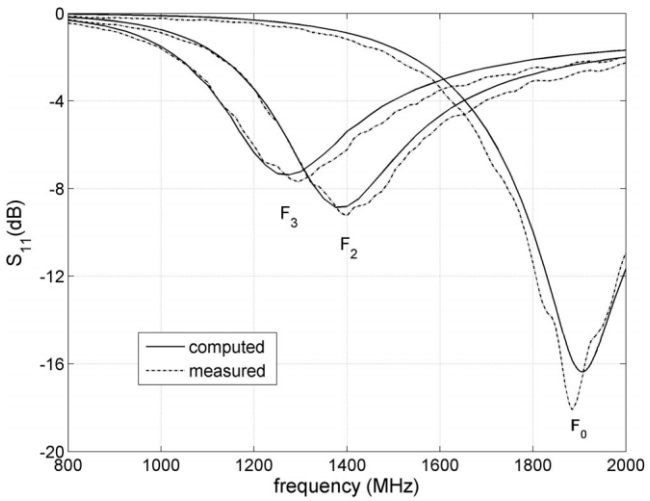

Figure 10 The measured and computed S_{11} for the *F* versions

ence of this antenna from the conventional ones is that the branch lengths are determined according to the special Fibonacci number sequence and their ratios are not constant. The proposed and conventional designs have been simulated by using the method of moments and compared in terms of the fundamental antenna parameters for two different geometries. The new antenna performs better and it is very effective in miniaturization than the other one. The antennas were also fabricated and measured for the comparisons and verification of the design.

REFERENCES

1. K. Falconer, Techniques in fractal geometry, Wiley, Canada, 1997.
2. M.F. Barnsley, Fractals everywhere, Academic Press, Massachusetts, 1993.
3. J.P. Gianvittorio and Y.R. Samii, Fractal antennas: A novel miniaturization technique, and applications, IEEE Antenn Propag Mag 44 (2002), 20–36.
4. C. Puente, J. Romeu, and A. Cardama, The Koch monopole: A small fractal antenna, IEEE Trans Antenn Propag 48 (2000), 1773–1781.
5. Y.C. Lee, J.S. Sun, and S.C. Lin, Wideband fractal printed monopole antennas, Microwave Opt Technol Lett 49 (2007), 561–564.
6. C. Puente, J. Romeu, R. Pous, J. Ramis, and A. Hijazo, Small but long Koch fractal monopole, Electron Lett 34 (1998).
7. S. R. Best, On the resonant behavior of the small Koch fractal monopole antenna, Microwave Opt Technol Lett 35 (2002), 311–315.
8. S.R. Best, On the resonant properties of the Koch fractal and other wire monopole antennas, IEEE Trans Antenn Propag 1 (2002), 74–76.
9. M. Ding, R. Jin, J. Geng, and Q. Wu, Design of a CPW-fed ultrawideband fractal antenna, Microwave Opt Technol Lett 49, (2007).
10. I.I.-K. Kim, J.G. Yook, and H.K. Park, Fractal-shape small size microstrip patch antenna, Microwave Opt Technol Lett 34 (2002), 15–17.
11. J.P. Gianvittorio and Y.R. Samii, Fractal Yagi antennas: Design, simulation, and fabrication, Microwave Opt Technol Lett 41 (2004), 375–380.
12. J.P. Gianvittorio and Y. Rahmat-Samii, Fractal element antennas: A compilation of configurations with novel characteristics, IEEE Antenn Propag Soc Int Symp 3 (2000), 1688–1691.
13. C. Puente, J. Romeu, R. Pous, and A. Cardama, On the behaviour of the Sierpinski multiband fractal antenna, IEEE Trans Antenn Propag 46 (1998), 517–524.
14. J. Romeu and J. Soler, Generalized Sierpinski fractal multiband antenna, IEEE Trans Antenn Propag 49 (2001), 1237–1239.
15. D.H. Werner and S. Ganguly, An overview of fractal antenna engineering research, IEEE Antenn Propag Mag 45 (2003), 38–57.
16. D.H. Werner, R.L. Haupt, and P.L. Werner, Fractal antenna engineering: The theory and design of fractal antenna arrays, IEEE Antenn Propag Mag 41 (1999), 37–58.
17. H. Rimili, O.E. Mrabet, J.M. Floc'h, and J.L. Miane, Study of an electrochemically-deposited 3-D random fractal tree monopole antennas, IEEE Trans Antenn Propag 55 (2007).
18. J.S. Petko and D.H. Werner, Miniature reconfigurable three-dimensional fractal tree antennas, IEEE Trans Antenn Propag 52 (2004).
19. J.K. Vinoy, K.J. Abraham, and K.V. Varadan, Fractal dimension and frequency response of fractal shaped antennas, In Proceedings of the IEEE Antennas and Propagation Society International Symposium, Columbus, OH, June 2003, pp. 222–225.
20. T. Koshy, Fibonacci and Lucas numbers with applications, Wiley, USA, 2001.
21. Supernec 2.7 Academic, Poynting Software Ltd., Available at: www.poynting.co.za.

SPARSE FACTORIZATION OF FINITE ELEMENT MATRICES USING OVERLAPPED LOCALIZING SOLUTION MODES

J.-S. Choi,[1] R. J. Adams,[1] and F. X. Canning[2]
[1] Electrical and Computer Engineering, University of Kentucky, Lexington, KY 40506-0046; Corresponding author: rjadams@uky.edu
[2] Simply Sparse Technologies, Inc., Morgantown, WV 26508

Received 21 August 2007

ABSTRACT: *Local-global solution (LOGOS) modes provide a computationally efficient framework for developing fast, direct solution methods for electromagnetic simulations. In this article, we demonstrate that the LOGOS framework yields fast direct solutions for finite element discretizations of the wave equation in two dimensions. For fixed-frequency applications, numerical examples demonstrate that the memory and CPU complexities of the proposed solver are nearly linear.* © 2008 Wiley Periodicals, Inc. Microwave Opt Technol Lett 50: 1050–1054, 2008; Published online in Wiley InterScience (www.interscience.wiley.com). DOI 10.1002/mop.23298

Key words: *finite element method; solver; sparse factorization; localizing*

1. INTRODUCTION

It has recently been observed that local-global solution (LOGOS) modes provide a useful framework for the development of fast, direct solutions of integral equation formulations of frequency-domain electromagnetic radiation and scattering problems [1-6]. In particular, overlapped, localizing LOGOS (OL-LOGOS) modes have been observed to provide a fast direct solution procedure with approximately $O(N)$ memory and $O(N \log N)$ CPU costs for fixed-frequency discretizations of integral equations [4]. In the following, "fixed-frequency" is used to refer to the situation in which the number of unknowns, N, used to discretize a given problem increases while the frequency remains fixed.

The purpose of this article is to demonstrate that the OL-LOGOS solution procedure also provides a sparse solver for finite element discretizations of the wave equation for transverse magnetic (TMz) polarization field problems. For fixed-frequency simulations, the memory and CPU costs of the OL-LOGOS solver are observed to scale nearly linearly with N. The OL-LOGOS factorization is also shown to provide an efficient strategy for computing the resonant frequencies of lossless structures.

2. TMz FEM SYSTEM DEFINITION

The z-directed electric field, E_z, associated with TMz polarized fields on a piece-wise homogeneous domain satisfies the two-dimensional Helmholtz equation [7, 8],

$$\nabla^2 E_z(x, y) + \varepsilon_r(x, y) k_0^2 E_z(x, y) = 0. \quad (1)$$

In (1), $k_0 = 2\pi f\sqrt{\varepsilon_0 \mu_0}$ is the wave number, and $\varepsilon_r(x, y)$ indicates the relative permittivity; the relative permeability is assumed to be unity. In the following numerical examples, ε_r is piecewise constant in the simulation domain (cf. Fig. 2).

Let Ω indicate the domain over which E_z is defined, and let Γ indicate the boundary of Ω. With a testing field E_z^a, the weak form of (1) can be written as [7, 8]

$$\int_\Omega \int (\nabla E_Z^a \cdot \nabla E_Z - k_0^2 \varepsilon_r E_Z^a E_Z) d\Omega - \int_\Gamma E_Z^a \hat{n} \cdot \nabla E_z d\ell = 0, \quad (2)$$